Contents lists available at ScienceDirect

Corrosion Science

Investigation of AISI 1040 steel corrosion in H$_2$S solution containing chloride ions by digital image processing coupled with electrochemical techniques

Alexsandro Mendes Zimer [a,1], Emerson Costa Rios [a,1], Paulo de Carvalho Dias Mendes [a,1], Wesley Nunes Gonçalves [b,2], Odemir Martinez Bruno [b,2], Ernesto Chaves Pereira [a,1], Lucia Helena Mascaro [a,*,1]

[a] Laboratório Interdisciplinar de Eletroquímica e Cerâmica (LIEC), Universidade Federal de São Carlos (UFSCar), Chemistry Dept., CP: 676, CEP: 13.565-905, São Carlos, SP, Brazil
[b] Instituto de Física de São Carlos (IFSC), Universidade de São Paulo (USP), Depto. Física, CP: 369, CEP: 13.560-970, São Carlos, SP, Brazil
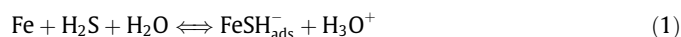
ARTICLE INFO

ABSTRACT

This paper presents a study of AISI 1040 steel corrosion in aqueous electrolyte of acetic acid buffer containing 3.1 and 31 × 10^{-3} mol dm^{-3} of Na$_2$S in both the presence and absence of 3.5 wt.% NaCl. This investigation of steel corrosion was carried out using potential polarization, and open-circuit and in situ optical microscopy. The morphological analysis and classification of types of surface corrosion damage by digital image processing reveals grain boundary corrosion and shows a non-uniform sulfide film growth, which occurs preferentially over pearlitic grains through successive formation and dissolution of the film.

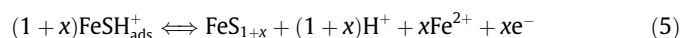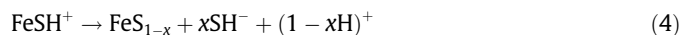© 2011 Elsevier Ltd. All rights reserved.

1. Introduction

Pipeline corrosion occurs due to the presence of aggressive species in hydrocarbon mixtures, such as sulfides, polysulfides, cyanides, nafthenic acids, nitrogen compounds, and/or oxygen compounds [1]. Dissolved sulfide species are common during the production and transportation of hydrocarbons in the oil industry, and as a consequence, steel pipelines become corroded and iron sulfide films are formed [2]. The iron sulfide film can both inhibit and accelerate the corrosion process, depending on the experimental conditions during oil transportation [3,4].

The physicochemical nature and thickness of iron sulfide films are also dependent on potential, and have, therefore, been extensively studied using electrochemical techniques [5–8]. Different sulfide species in the solution exist as a function of pH. In agreement with the pH-sulfide equilibrium diagram, at pH > 5.5, the main species is HS$^-$ [5,6] leading to a thick sulfide film. If the solution pH is lower than 5.5, the main species is H$_2$S$_{aq}$. In the latter case, Ma et al. [3] and Shoesmith et al. [7] have proposed that the corrosion process occurs as follows:

$$Fe + H_2S + H_2O \Longleftrightarrow FeSH^-_{ads} + H_3O^+ \tag{1}$$

$$FeSH^-_{ads} \Longleftrightarrow Fe(SH)_{ads} + e^- \tag{2}$$

$$Fe(SH)_{ads} \rightarrow FeSH^+ + e^- \tag{3}$$

According to these authors [7,8], the FeSH$^+_{ads}$ species is incorporated in the sulfide film as mackinawite (FeS$_{(1-x)}$) layers (Eq. 4) or pyrrhotite (FeS$_{(1+x)}$) if the solution pH is between 3.0 and 5.5, leading to a thin film over the surface:

$$FeSH^+ \rightarrow FeS_{1-x} + xSH^- + (1 - xH)^+ \tag{4}$$

$$(1 + x)FeSH^+_{ads} \Longleftrightarrow FeS_{1+x} + (1 + x)H^+ + xFe^{2+} + xe^- \tag{5}$$

At solution pH values lower than 2.0, the species described in Eq. (3) is hydrolyzed to produce dissolved Fe^{2+} [3,8].

$$FeSH^+ + H_3O^+ \Longleftrightarrow Fe^{2+} + H_2S + H_2O \tag{6}$$
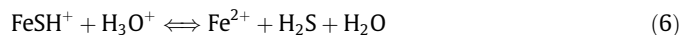
Mackinawite, at low H$_2$S concentration, i.e. ⩽0.04 mmol dm^{-3} [3], initially accelerates the corrosion instead of inhibiting it. However, for longer exposition times, mackinawite is converted to pyrite (cubic FeS$_2$), pyrrhotite (FeS$_{(1+x)}$) or troilite (stoichiometric pyrrhotite, FeS), which can inhibit the corrosion process [3,4,9].

A computational approach to predicting the formation of sulfide films using stability diagrams has been presented by Anderko and Shuler [10]. These authors have proposed that the FeSH$^+$ ion or Siderite (FeCO$_3$) in the presence of O$_2$ are always precursors to sulfide films. In this case, the second step is the formation of iron monosulfide followed by amorphous FeS, mackinawite and

* Corresponding author.
  E-mail address: lmascaro@dq.ufscar.br (L.H. Mascaro).
[1] Tel.: +55 16 3351 9452; fax: +55 16 3361 5215.
[2] Tel.: +55 16 3373 8728; fax: +55 16 3373 3365.

pyrrhotite. In a third step, the transformation to pyrite may occur through greigite (Fe_3S_4) and/or marcasite (orthorhombic FeS_2) and could involve any monosulfide from the previous steps.

Although the behavior of iron in sulfide solution has been investigated for many years, several points remain under discussion and, as such, other approaches have been proposed to investigate them. In 2005, Choi and Kim proposed the use of micrograph quantitative analysis [11] to investigate the corrosion process, rather than electrochemical methods. The observation of a corroded surface can provide important information about the corrosion process. Even simple imaging techniques, such as the comparison of corroded surfaces to determine the grain size and correlate these with the material history [12], or the extrapolation of structure through three-dimensional models [13] can gather knowledge of the system. Oliveira et al. have investigated the corrosion resistance of sputter-coating W-Ti-N films on steel substrates, in salt spray, using image analysis. The evolution pit size growth and its spatial distribution have been quantified to account for corrosion on the surface [14]. Punckt et al. have investigated stainless steel corrosion and used spatial statistics to predict interactions between metastable pit spots during nucleation [15] and concluded that they interact with each other. This proposition was corroborated by Lopes de La Cruz et al., who used a different analysis procedure [16,17]. Image evaluation with chemometric strategies were presented by Pereira et al. [18], applied in the quality control of paints. The discrimination for the primers evaluated was in accordance with the degradation processes related to accelerated laboratory tests.

Considering that which has been exposed above, this paper aims to study the corrosion of AISI 1040 steel in aqueous solution containing H_2S, which exists at pH 4.5, and the effect of the presence of chloride in the process using a different approach: time series image acquisition and quantitative analysis coupled with conventional electrochemical techniques.

2. Experimental

A stock solution at 311×10^{-3} mol dm^{-3} of Na H_2S was prepared by the dissociation of $Na_2S.9H_2O$ (Synth). Buffered acetic acid solution/sodium acetate (pH 3.5) (Mallinckrovodt)/(Merck) was used, with sulfur species at 3.1 or 31×10^{-3} mol dm^{-3}. The presence of Cl^- was investigated by the addition of 3.5 wt.% (0.6 mol dm^{-3}) NaCl (J.T. Baker) to the solution. From the pH-sulfide equilibrium diagram it can be observed that the main species present, at pH < 5.5, is undissociated H_2S_{aq} [6].

The AISI 1040 steel samples (Sanchelli) were used as received. In addition, we also studied one AISI 1020 steel plate to determine the pearlite–ferrite surface area ratio using the procedure established by the ASTM E 1382-97 standard [19]. In the metallographic studies, these two samples were etched for 10 s in fresh Nital solution [20]. The cylindrical AISI 1040 steel samples have a cross-sectional area of 0.709 cm^2 with 9.5 mm diameter. They were embedded in an epoxy resin to expose only the cross section in the working electrode.

Prior to use, the electrodes were abraded with sandpaper up to 1200-grit, then polished with alumina 25 μm, and finally degreased in acetone for 3 min in an ultrasonic bath.

To perform the in situ image acquisition, the electrodes were mounted in a flat-bottom electrochemical cell, which was built in
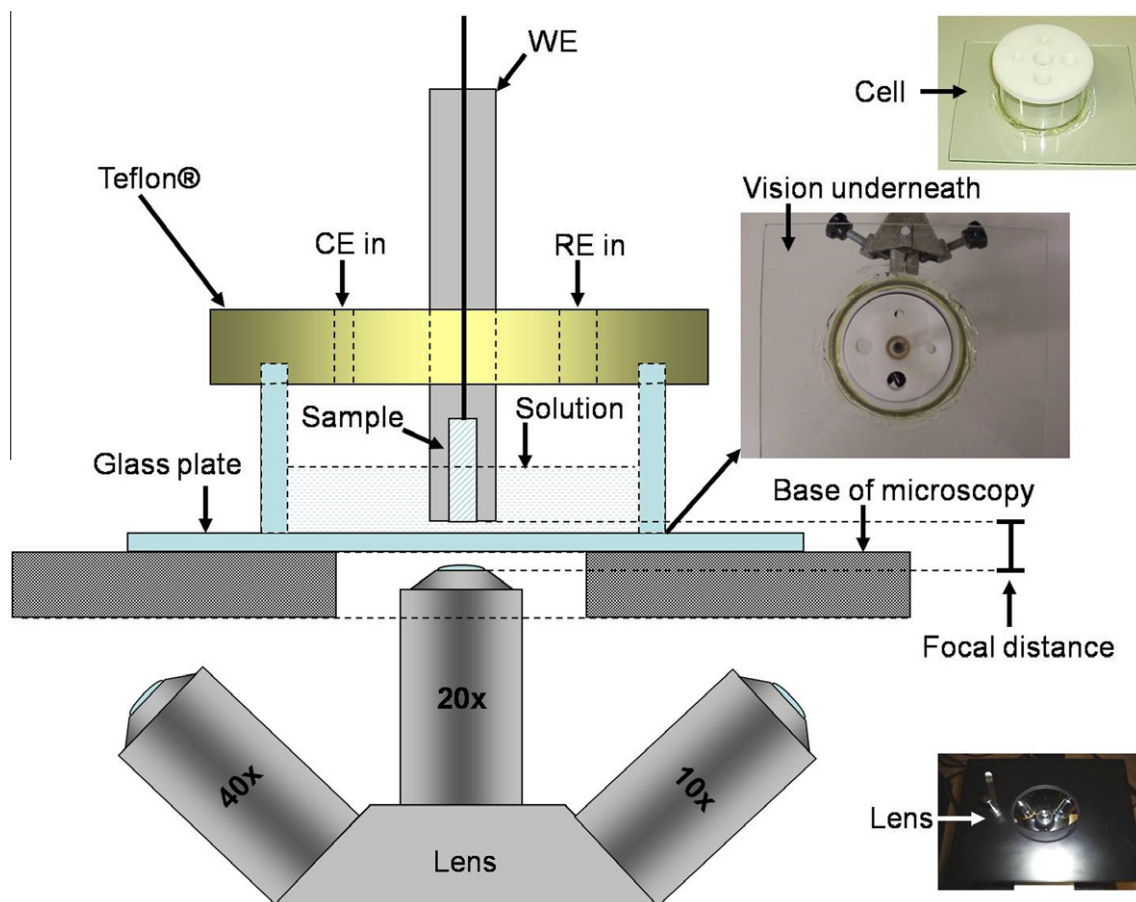

Fig. 1. Schematic diagram describing the electrochemical cell and the base of the inverted optical microscope.

an inverted optical microscope (Opton model TNM-07T-PL), as depicted in Fig. 1. The images were collected with a magnification of 200× using the program Scope Photo® 1.0. As shown in Fig. 1, this setup allows simultaneous optical measurements for electrochemical experiments. All electrochemical measurements were carried out using an Autolab model PGSTAT 30. The counter electrode was a platinum wire and the reference electrode was an Ag/AgCl/KCl (sat.). After a stable open-circuit potential, E_{oc}, was reached, a polarization curve was accomplished using $v = 0.1$ mV s^{-1} in a potential range from 200.0 mV more negative than E_{oc}, up to 200 mV more positive than E_{oc}. The image acquisition rate used was 0.1 frames s^{-1} to follow E_{oc} stabilization and 0.5 frames s^{-1} during the polarization curves.

Two different procedures were used in the image analysis. First, the micrographs (1280 × 1024 pixels) were scaled to 340.0 × 272.0 µm real dimension. Following this, they were binarized, setting the threshold in the first image of the video in such a way that the pearlitic regions were selected as bit zero [24], and then binarized. With this procedure, comparing the black areas (bit 0) and the white areas (bit 1), it is possible to determine which part was corroded and to quantify this as a function of time or potential. A flowchart of this procedure is presented in Fig. 2, left path.

When the threshold was set in the first image of the video, i.e. at $t = 0$ s, it was observed that very few pearlitic regions were corroded with sulfide film formation, and only these grains appear in the image as dark regions. Otherwise, ferrite together with uncorroded pearlitic grains appear as clear regions at this initial stage. As the corrosion process occurs, pearlitic grains react and are then also observed as dark regions. We therefore decided to follow the corroded area change in these experiments as a consequence of the conversion of clear pearlitic unreacted grains into dark corroded ones due to sulfide film formation over these regions only. It is important to stress that, for solutions containing Cl$^-$ ions, both ferritic and pearlitic grains corrode and this the final state of

the surface is completely dark, i.e. sulfide film formation extends over the whole surface.

Alternatively, as in situ microscopic observation allows the collection of three-channel real-color images, complementary information to that obtained with binarized images can be extracted using color images. A flowchart of the color image processing used is presented in Fig. 2, right path. A Java application was developed to select a polygon pixel of interest and to analyze the changes at that particular pixel's group in a video sequence. In the evaluation of the video sequence it is an important to ensure that there is no shift or rotation in the pixels of the video sequence. This process is also known as image registration in the field of image processing. Consider a pixel p_a at a position x,y in frame t_a; our evaluation process ensures that p_a corresponds to the same material region of the pixel p_b at position x,y in the frame t_b. This analysis was carried out for all frames of the video to evaluate the whole video sequence. The mathematical basis for this process is the phase correlation property of the Fourier Transform, and detail about its implementation can be found in the work of Reddy and Chatterji [21].

The color image processing presented in Fig. 2 shows an image region visually interpreted as a pearlitic grain, which represents the region of interest "P". To improve the result liability, six regions were selected, i.e. six pearlitic grains in each experiment were used to validate this method. For each P group the chromatic components of the pixels were calculated. Two different color models were considered in this study: the RGB (red, green and blue), and HSI (hue, saturation, and intensity) models. RGB is based on the trichromatic vision model originally proposed by Helmholtz in the 19th century [31–33]. It is an additive color model that uses the primary colors red, green and blue, which stimulate each of the three human retinal photoreceptors (response cones for long, medium and short wavelengths). The RGB model presents one byte (0–255) to represent each of the R, G and B components.
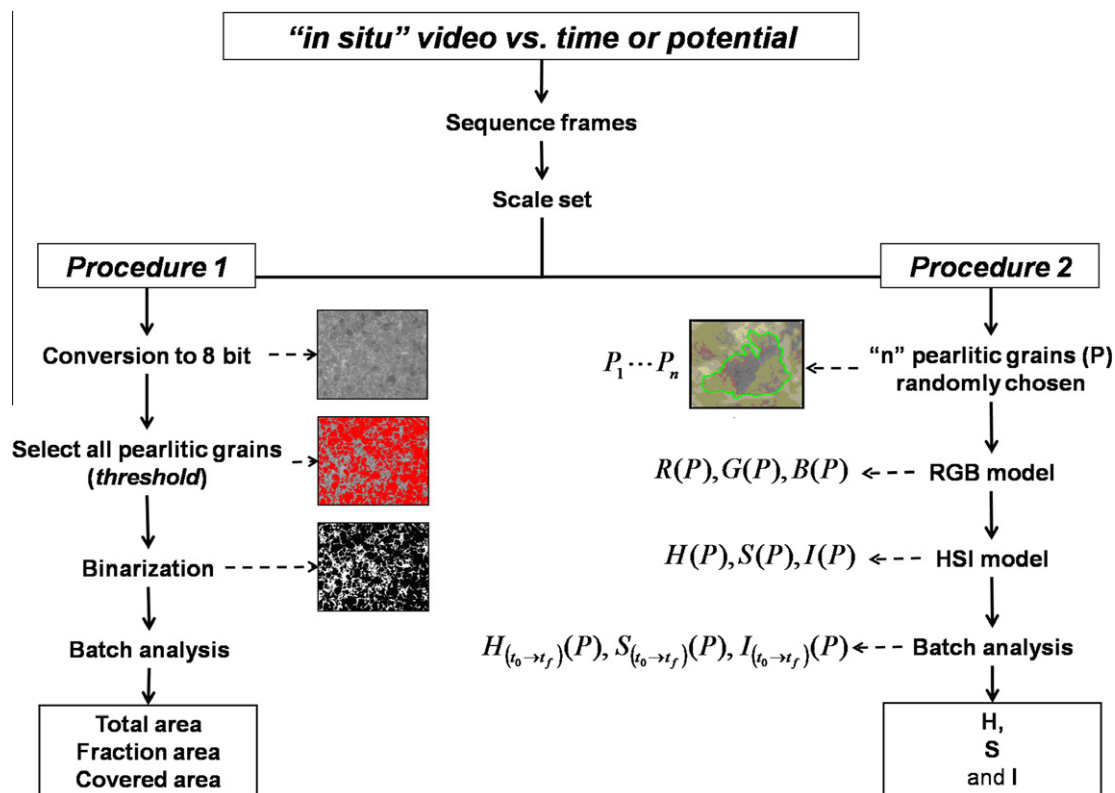

Fig. 2. Flowchart used in digital image processing of the corroded samples using binarized and color images.

Considering the video as a sequence of images represented by a bi-dimensional function in time (t): $I_t(x,y) = [R_t(x,y)G_t(x,y)B_t(x,y)]$, then the mean value of R, G and B components between the pixels in each region of interest "P" (for one pearlitic grain, randomly chosen) can be computed by:

$$R_t(P) = \frac{1}{n_P} \sum_{(x,y) \in P} R_t(x,y)$$

$$G_t(P) = \frac{1}{n_P} \sum_{(x,y) \in P} G_t(x,y) \qquad (7)$$

$$B_t(P) = \frac{1}{n_P} \sum_{(x,y) \in P} B_t(x,y)$$

The RGB representation was converted to the HSI model. This model was proposed to make the description of colors natural and intuitive for human beings. The HSI model separates the intensity I from information of color (H – hue, and S – saturation). Therefore, the analysis of how the color of the "P" region changes can be easily carried out by following the changes in the hue values. Using literature data [2] concerning the color of different sulfide films, we related their colors with changes that occur during the corrosion process. The color space conversion from RGB to HSI color space is given by:

$$H = \begin{cases} \theta, & \text{if } R \leqslant G \\ 360 - \theta, & \text{otherwise} \end{cases}$$

$$\theta = \cos^{-1}\left\{ \frac{0.5[(R-G)+(R-B)]}{[(R-G)^2 + (R-B)(G-B)]^{0.5}} \right\}$$

$$S = 1 - \frac{3}{R+G+B}[\min(R,G,B)] \qquad (8)$$

$$I = \frac{(R+G+B)}{3}$$

The H, S and I channels can be computed for the region of interest "P" in the same way as for the RGB model, and the results of mean values of six "P" regions were presented as a graph of H, S and I channels vs. time.

3. Results and discussion

In order to perform image analysis and to validate the procedure, we first compared two different steel samples, AISI 1020 and 1040, with different amounts of pearlitic phase. These images are presented in Fig. 3. As described in the literature [22], carbon steel is composed of both ferrite and pearlite grains. After metallographic etching for 10 s. in fresh Nital solution [20], it was observed that the pearlitic regions became dark. We then calculated the dark area and related it with the pearlitic phase. It was calculated as 28 ± 4% for AISI 1020 (Fig. 3a) and 96 ± 2% for AISI 1040 (Fig. 3b). These results are in agreement with results published in the literature [23], although they are higher than expected considering the samples used here were not annealed. After this test, we chose the AISI 1040 steel due to its higher content in the pearlitic phase, which eases the observation of surface changes. Image analysis can provide access to other important information about surface composition. AISI 1040 steel is composed of both ferrite and pearlite grains, the latter being composed of cementite (Fe_3C) alternated to α-iron [22]. It has been established in the literature [22] that these structures are easy to separate as α-iron has a lamellae morphology, which can be observed in Fig. 3 (insert). As a consequence, anodic and cathodic regions can form among these lamellas, and thus, under some experimental conditions, accelerate corrosion damage [24]. Moreover, the metallic heterogeneities could lead to a local corrosion process that is influenced by the steel-type constituent of the samples [22].

First, we investigated the behavior of steel exposed to 3.1×10^{-3} mol dm^{-3} of H_2S at pH 4.5 under open-circuit conditions using color images. In agreement with the pH-sulfide equilibrium diagram, at this pH value, the main species is H_2S_{aq} [5,6]. The purpose of this investigation was to follow the corrosion on the surface in this aggressive solution. In Fig. 4a, the surface is observed just after immersion, whereas Fig. 4b represents the situation after 10 min. In image 4b it can be observed that some regions on the surface became slightly brownish, which could be related to the early adsorption of sulfur and the growth of a sulfide film. In Fig. 4c, measured after 60 min of exposition to the solution, the same regions reveal grain boundary corrosion. These grains, observed as clear and dark areas, correspond to ferrite and pearlitic regions, respectively.

In a second experiment, we added 3.5 wt.% Cl$^-$ (0.6 mol dm^{-3}) to the solution (Fig. 4d), which was also measured after 60 min of immersion. In this case, a better definition of the grain boundary corrosion was observed as compared to the previous experiment, as seen in Fig. 4c, and this was, expected due to the presence of chloride in the solution.

Following E_{oc} measurements, to perform accelerated corrosion experiments the electrodes were polarized from a level of 200.0 mV more negative than the corrosion potential (E_{corr}) up to a level of 200.0 mV more positive. Prior to these experiments, the potential was followed for 60 min until E_{oc} became stable and this was used as the criterion to start those measurements. At the same time as the potential sweep, images were collected during the anodic polarization using 0.5 frames s^{-1} as acquisition rate.

A comparison between the characteristics of corrosion measurements in sulfide and chloride solutions by polarization curves
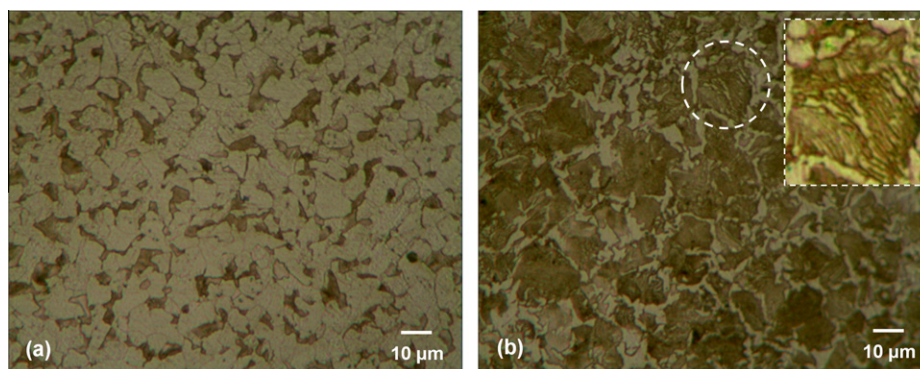

Fig. 3. Metallographic results of AISI 1020 (a) and AISI 1040 (b) carbon steel samples. The samples were etched for 10 s. in fresh Nital solution. (insert) Magnification of the selected region of AISI 1040 steel showing the pearlitic phase.
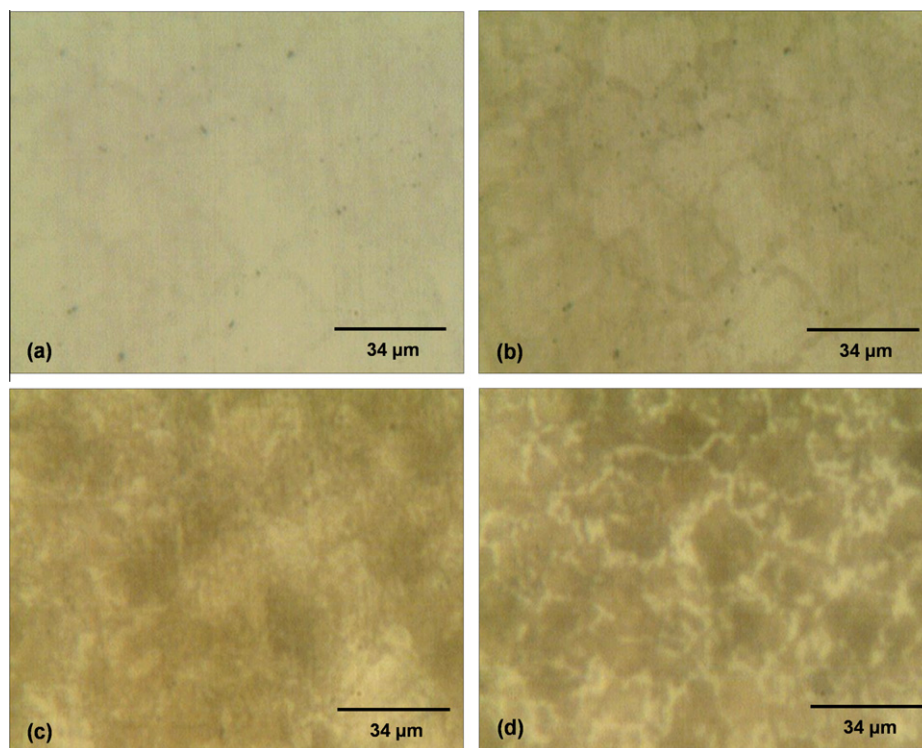
Fig. 4. In situ continuous microscopy observation of AISI 1040 steel until E_{oc} stabilization in 3.1×10^{-3} mol dm^{-3} of H$_2$S without NaCl (a–c) and with NaCl (d). Snapshots at 0 (a), 10 (b) and 60 (c and d) minutes. Full video sequence is available on site.

are presented in Fig. 5, and the important parameters measured from these curves are summarized in Table 1.

In the presence of chloride ions it can be observed that the E_{corr} shifts to a value that is 105 mV more negative. The same effect is observed to increase the H$_2$S concentration to 31×10^{-3} mol dm^{-3} in the presence of chloride ions, showing that this solution presents the highest possibility of thermodynamic corrosion among all the conditions investigated. The corrosion current (i_{corr}) in 3.1×10^{-3} mol dm^{-3} sulfide solution obtained by extrapolation of the cathodic and anodic Tafel lines is 220.0 μA cm^2, which is higher than those (i_{corr} = 36.5 μA cm^2) observed in the same solution with chloride ions. In this sense, it was expected that the corrosion rate
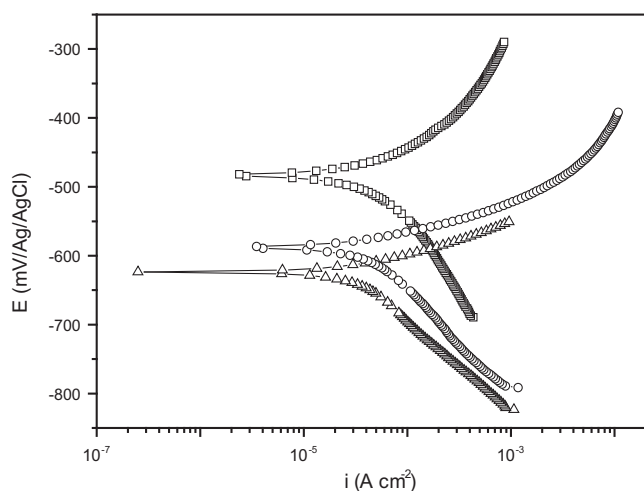
Table 1
Tafel parameters from polarization curves of Figure 5.

Parameters	Measurements		
	H$_2$S 100 ppm	H$_2$S 100 ppm + Cl$^-$	H$_2$S 1000 ppm + Cl$^-$
E_{oc}/mv (vs. Ag/AgCl)	−496	−597	−625
E_{corr}/mv (vs. Ag/AgCl)	−483	−588	−623
i_{corr}/μA cm^{-2}	220.0	36.5	29.5
V_{corr}/mm year^{-1}	3.60	0.59	0.48
R_p/Ω cm^2	422.8	386.2	489.9

(v_{corr}) for the latter condition would be higher than that of the former. However, the opposite behavior was observed, i.e. v_{corr} is drastically reduced in Cl$^-$ solutions. This fact could be associated with the initial fast metal dissolution, which favors sulfide film formation over the metal surface as proposed in the literature [25].

The images collected during the anodic polarization curves in 3.1×10^{-3} mol dm^{-3} of H$_2$S at pH 4.5 are presented in Fig. 6. In these images, it is clear that the whole surface has been corroded, but with different rates as the identification of grain boundaries is possible. Moreover, film formation over the pearlitic grains is typically characterized by the bluish color of sulfide films [26]. Using color metallographic experiments [27], it was proposed that the color is sensitive to differently oriented crystallites in a polycrystalline material. In addition to the bluish regions, grains that were brownish in color were also observed. We propose that these changes between brownish and bluish regions over the pearlitic grains could come from the formation and thickening of mackinawite (dark brown). However, the surface changes in color occur only over pearlitic grains, and the mackinawite formation then initially accelerates the process of corrosion instead of inhibiting it [3]. Of course, its thickness is not enough to reduce the corrosion rate as observed in comparison to the data presented in Table 1. As only pearlitic grains change color, one can conclude that

Fig. 5. Polarization curves obtained for AISI 1040 steel in 3.1×10^{-3} mol dm^{-3} of H$_2$S (□), 3.1×10^{-3} mol dm^{-3} of H$_2$S solution 3.5 wt.% Cl$^-$ (0.6 mol dm^{-3}) (○), and 31×10^{-3} mol dm^{-3} of H$_2$S and Cl$^-$ same solution (△).
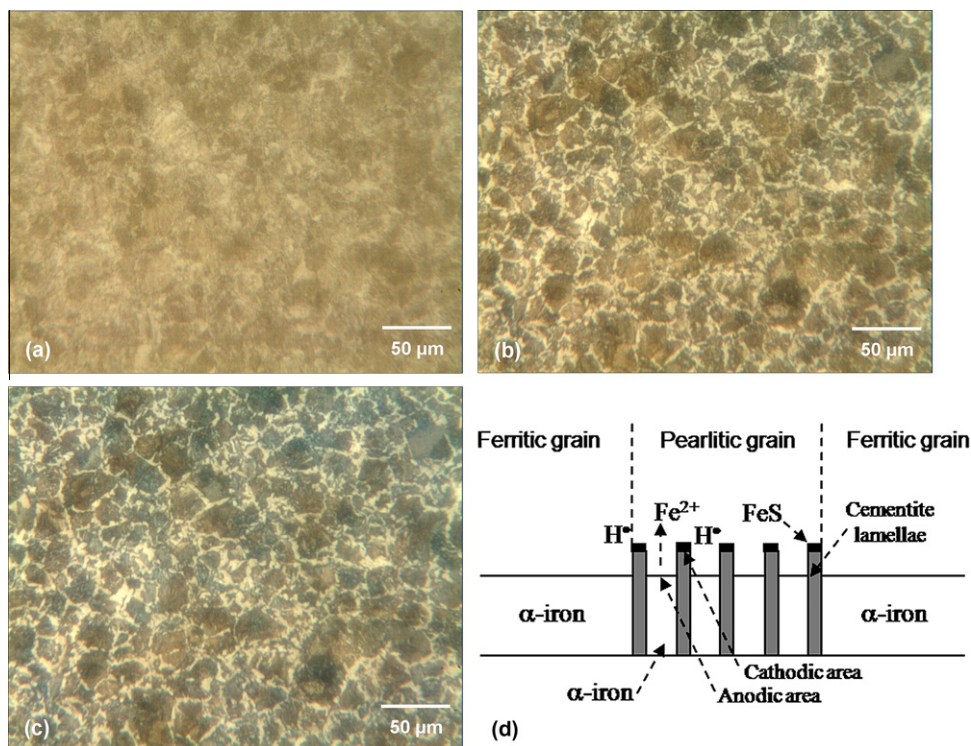
Fig. 6. In situ microscopy observation of AISI 1040 steel during polarization in 3.1×10^{-3} mol dm^{-3} of H$_2$S. Snapshots measured at $\Delta E = 36.1$ mV (a), $\Delta E = 134.1$ mV (b) and $\Delta E = 156.5$ mV (c). All potentials measured vs. E_{oc}. (d) Schematic representation of the changes in pearlitic grain due to local increase in pH value over these regions [24]. Full video sequence is available on site.

non-uniform film formation occurs over the AISI 1040 steel surface, which is in opposition to previously published papers [3,25,28,29]. In these papers, the authors made their conclusions that uniform sulfide film formation occurs based only on the results of electrochemical experiments. From a different point of view, our data are in agreement with measurements by Huang and Lee [24] that propose, using EDS data, that a non-uniform sulfide film only forms over pearlitic grains. One possible mechanism to explain the non-uniformity of the film is that cementite acts as a cathode while metal dissolution occurs at the α-iron part of the pearlite grain, leading to an increase in the local pH value, which in turn results in a preferential deposition of FeS film over these regions [24], as schematically represented in Fig. 6d.

The influence of chloride ions on sulfide film formation is observed in Figs. 7a–f. It is possible to detect regions with different colors: brownish and bluish. The inset of Fig. 7 follows specific grains during the corrosion test and reveals a new experimental fact; as can be observed, its color is initially brown (a) changing to bluish (Fig. 7c), brown (Fig. 7d), until finally becoming blue again (Fig 7e). Therefore, a different proposition must be considered compared to those data measured in Fig. 6. One possibility is film dissolution and regrowth [30]. In a solution with pH 4.5, it has been proposed [6] that metal dissolution is favored under open-circuit potential. Otherwise, under anodic polarization, such as that used in Figs. 6 and 7, sulfide formation can be observed due to potential polarization to more positive values than E_{oc}, and this is supported by the Pourbaix diagram for the ternary system iron–sulfide–H$_2$O diagrams [6]. The dissolution of the sulfide film is also supported by the data of Veloz and Gonsález [25], which propose that Cl$^-$ ions are able to prevent the formation of sulfide films due to their competitive adsorption with these species, and, therefore, the process starts again.

At higher potentials, as seen in Fig. 7f, the surface is too dark to allow the detection of changes in color. At this point it can

observed that, at 180.6 mV more positive than E_{oc}, sulfide film formation occurs over the entire surface, i.e. both pearlitic and ferritic grains are covered. This fact could explain the low value of v_{corr} presented in Table 1, as these new sulfide species are more resistant to corrosion. At this stage the conversion of mackinawite (black) to pyrrhotite (brown) or in stoichiometric pyrrhotite (black) together with amorphous FeS, iron sulfide species could be expected from color analysis and data available in the literature [4,10].

As it was possible to monitor the changes over the entire surface during the potentiodynamic corrosion experiments, we first analyzed its behavior using binarized images (Fig. 2), which are presented in Fig. 8, together with the anodic polarization curves. As expected for these experiments in the absence of Cl$^-$ ions (Fig. 8a), no oscillation in the covered area is observed and the images are up to 93% dark, which is in agreement with the surface composition presented in Fig. 3b. This fact indicates that, under this condition, only the pearlitic grains are corroded. Moreover, an induction period with a low rate of formation of corrosion products was observed, i.e. the surface remained in its initial state until $\Delta E = 50.0$ mV, which could be related to a slow corrosion process. Finally, for ΔE values from 50.0 mV up to 125.0 mV, most of the surface is covered by corrosion products (80% dark surface) and after this value the corrosion rate decreases again, until 93% of the surface is covered.

In the presence of Cl$^-$ ions in the solution, as shown in Fig. 8b, a completely different behavior is observed. First, at the end of experiment, the whole surface becomes dark, indicating that both pearlitic and ferritic grains are covered by corrosion products. For the highest H$_2$S concentration, 31×10^{-3} mol dm^{-3} in the presence of Cl$^-$, as shown in Fig. 8c, similar behavior is observed; however, the time to cover the surface by corrosion products is shorter: $\Delta E = 130.0$ mV (Fig. 8b), compared to $\Delta E = 150.0$ mV. This result is expected, as the latter solution has strong passivating properties.
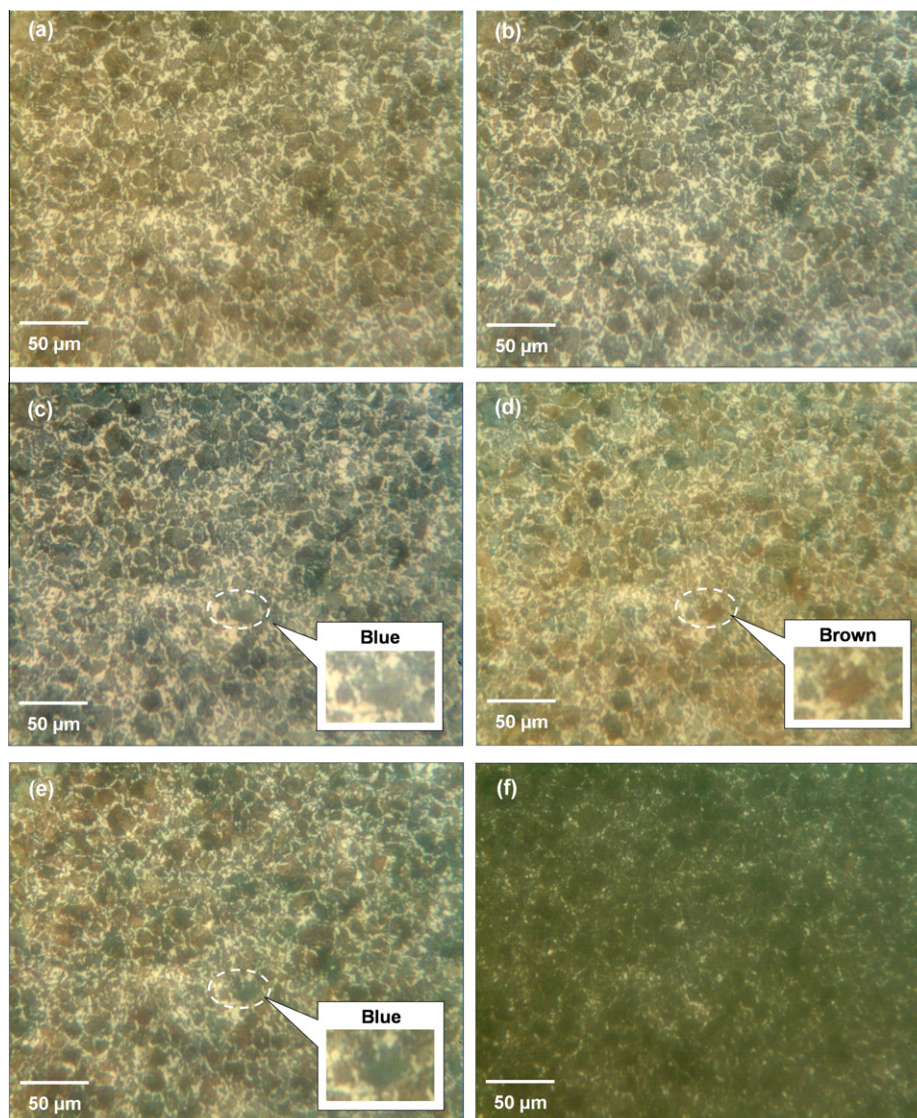
Fig. 7. In situ microscopy observation of AISI 1040 steel during polarization in 3.1×10^{-3} mol dm^{-3} of H$_2$S with NaCl in acetate buffer (pH 4.5). Snapshots at $\Delta E = 36.3$ mV (a), $\Delta E = 54.4$ mV (b), $\Delta E = 72.7$ mV (c), $\Delta E = 90.8$ mV (d), $\Delta E = 108.9$ mV (e) and $\Delta E = 180.6$ mV (f). All potentials measured vs. E_{oc}. Full video sequences are available on site.

These propositions are also supported by those data presented in Table 1, where it can be observed that v_{corr} and I_{corr} decrease in solutions containing Cl$^-$.

Therefore, following the reaction using in situ microscopy experiments, it was possible to achieve local surface information that has not been described before in the literature using real-time successive surface image acquisition experiments. Then, as described above, an oscillation in color was detected over the surface, as shown in Figs. 6–8, but the current signal does not detect such behavior. This means that the current measured during the polarization curves is, as expected, an average value of the surface modifications. Otherwise, in situ microscopy measurements are useful in providing local information revealing non-uniform changes on the surface during the corrosive process. Following this reasoning, the most important aspect of Fig. 8 is the covered area oscillation observed in Fig. 8b and c, i.e. for those experiments in the presence of chloride ions. Such behavior occurs at approx. $\Delta E = 56.0$ and 98.0 mV, respectively, in relation to local variations (Fig 8b) or between $\Delta E = 67.0$ and 106.0 mV (Fig. 8c). Alternating colors between brown and blue over a specific pearlitic grain are not observed in Fig. 6, in which only a single change from brown to blue occurs.

As observed in Fig. 7, for those experiments in Cl$^-$ solution the situation is different. To discuss this behavior, colored images were used instead of binarized ones following the image treatment described in Fig. 2, right path. In Fig. 7, it was possible to observe that, during corrosion experiments, the color of some regions on the surface changed from brownish to bluish, and this behavior is repeated. During mackinawite formation in the presence of Cl$^-$ ions, this film could be dissolved, as proposed by Veloz and Gonzalez [25]. In a second step, the mackinawite film is formed again [28] and the process restarts. This proposition is supported by Fig. 9, in which the hue, saturation and intensity measured for six specific grains in the surface using the HSI color model [11,31–33] can be observed. Hue (H) is a property associated with the predominant wavelength in the combination of several waves in the visible region of the spectrum – therefore, in the simplest case, the color of a compound. Saturation (S) expresses the purity of the hue, in other words, the degree of mixing of the original hue with white light, and the intensity (I) represents the concept of luminous brightness of the radiation. The time variation of H, S, and I parameters for those samples measured in the absence (Fig 8a) and presence (Fig. 8b) of Cl$^-$ ions are presented in Fig. 9a and b, respectively. It can be observed that in this figure the hue and
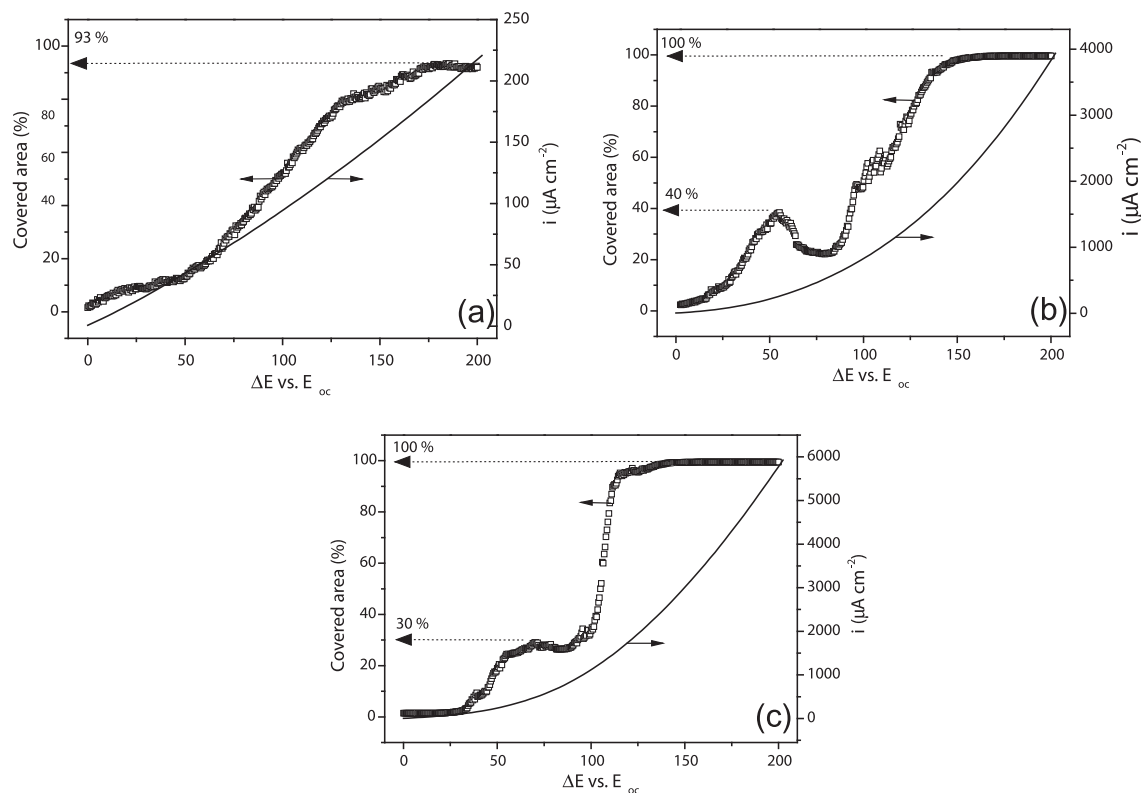
Fig. 8. Polarization curve as a function of the covered area calculated using ImageJ software on the full video sequence of the corrosion process. Acquisition rate 0.5 frames s^{-1}. Electrode of AISI 1040 steel in 3.1×10^{-3} mol dm^{-3} of H$_2$S, without NaCl (a), with NaCl (b) and in 31×10^{-3} mol dm^{-3} of H$_2$S solution with NaCl (c).

saturation for those samples measured in the presence of Cl$^-$ ions show an oscillation, which matches with those observed in Fig. 8b. Therefore, the oscillation in the binarized images (Fig. 8b) is associated with a color change (Fig. 9b). It is important to emphasize that such oscillations were not observed for samples investigated in the absence of Cl$^-$ ions (Figs. 8a and 9a). The HSI model in Fig. 9b shows that the hue presents maximum and minimum peaks at $\Delta E = 73.0$ and 108.0 mV more positive than E_{oc} As such, this result occurs quite close to ΔE values at which the oscillation in the binarized images, as shown in Fig. 8b, occurs and we therefore propose that both are associated with the same experimental facts. The oscillation in hue values is associated to a color change, as presented in Fig. 7. The decrease in saturation in Fig. 9b, which occurs at the ΔE as the hue change occurs, could be associated to the fact that, after the color (hue) changes, the new color (hue) is no longer

a pure color but a mix of different colors. Such chromatic changes could be associated to the formation of mixed sulfide films [2,28] and their conversion [3,4] to different forms or even to a process of dissolution/regrowth. Literature data demonstrates that mackinawite has a black color, pyrrhotite is brown, stoichiometric pyrrhotite (troilite) is black, and marcassite and pyrite are yellow [4]. As such, the sulfide film conversion between these species is one possibility to explain the oscillation in the hue values, i.e. mackinawite is converted to more stable sulfide species, such as troilite and pyrite [10], at low quantities during the mackinawite thickening process. Such phase formation and conversion could explain the mixture of colors indicated by the saturation changes in Fig. 9b. However, a second event observed in Fig. 9b must be considered; if the observed process (corresponding to the experiment presented in Fig. 7) is related to sulfide film conversion, it
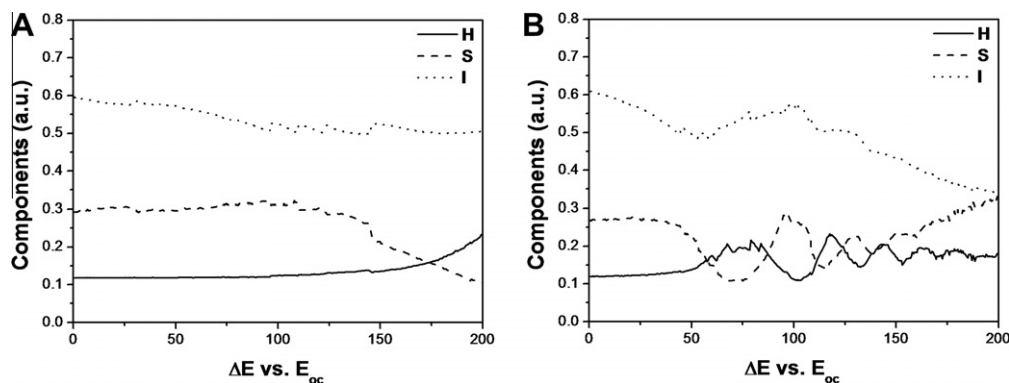

Fig. 9. Representation of the specific pixel region as a function of time during the polarization experiments corresponding to the pearlitic grains using the HSI color model: Hue (solid line), Saturation (dash line) and Intensity (dot line). Experiment in 3.1×10^{-3} mol dm^{-3} of H$_2$S (a) relative to Fig. 6, and in 3.1×10^{-3} mol dm^{-3} of with Cl$^-$ ions (b) corresponding to Fig. 7. ΔE vs. E_{oc}.

should be expected to occur only once. However, the oscillations in hue and saturation occur several times, at ΔE = 102.0, 133.0, 153.0, 170.0 and 186.0 mV. In our opinion, this behavior supports the process of dissolution/regrowth. Following this reasoning, in the absence of Cl^- ions, as shown in Fig. 9a, no oscillation in either hue or saturation is observed. The only change that occurs is the darkening of the surface, at ΔE = 110.0 mV, which is associated to an increase in hue values and a decrease in saturation. Instead, it is clear from Fig. 9b that it occurs several times, decreasing in intensity, and it seems to us that only the processes of dissolution and regrowth could explain such results. Moreover, the I coordinate of the HSI system decreases considerably, indicating that the surface, as a whole, becomes dark due to the formation of amorphous FeS together with other, more stable, sulfide species.

In summary, image analysis can be used as a complementary technique alongside electrochemical techniques. This first experimental tool offers information about the local corrosion process occurring on the surface, which can be used together with electrochemical data. Additionally, even using binary images and analyzing all the pixels on the surface, this information is sensitive to local changes on the surface, as local changes can be detected, i.e. specific regions can be investigated using colored images under different coordinate systems to support the experimentalist conclusions.

4. Conclusion

The use of in situ optical microscopy imaging as a function of the applied potential (or time) during a corrosion experiment has been presented here. This method is useful for the study of corrosion in situ, and this has made possible the observation of sequential images of corrosive processes, such as grain boundary corrosion and even the formation of initial stages of sulfide films for electrodes submitted to anodic polarization. The current signal measured in such experiments loses the local events that occur on the surface. Additionally, in situ images, such as those presented in this study, offer local information, revealing non-uniform changes on the surface during the corrosive process and even phase transformation.

Using the approach described above, it was observed that, with AISI 1040 steel in 3.1×10^{-3} mol dm^{-3} of H_2S aqueous solution with pH 4.5, sulfide film formation was detected over pearlitic grains. By contrast, in a solution of 3.1×10^{-3} mol dm^{-3} in the presence of 3.5% w/w of chloride ions, film formation occurs over both pearlitic and ferritic grains. Moreover, the experiments show oscillatory behavior in both binarized and colorized images, as a function of the potential, and we believe that the processes of dissolution and regrowth could explain such behavior.

Acknowledgments

References

[1] S. Mattar, L.F. Hatch, Chemistry of Petrochemical Processes, second ed., EUA, 2000.
[2] C. Azevedo, Failure analysis of a crude oil pipeline, Eng. Fail. Anal. 14 (2007) 978–994.
[3] H. Ma, X. Cheng, G. Li, S. Chen, Z. Quan, S. Zhao, L. Niu, The influence of hydrogen sulfide on corrosion of iron under different conditions, Corros. Sci. 42 (2000) 1669–1683.
[4] Z.F. Yin, W.Z. Zhao, Z.Q. Bai, Y.R. Feng, W.J. Zhou, Corrosion behavior of SM 80SS tube steel in stimulant solution containing H_2S and CO_2, Electrochim. Acta 53 (2008) 3690–3700.
[5] D.W. Shoesmith, M.G. Bailey, B. Ikeda, Electrochemical formation of mackinawite in alkaline sulphide solution, Electrochim. Acta 23 (1978) 1329–1339.
[6] M. Pourbaix, Atlas of electrochemical equilibria in aqueous solution, second ed., Pergamon Press, Texas, Houston, 1974.
[7] D.W. Shoesmith, T.E. Rummery, M.G. Bailey, D.G. Owen, Electrochemical formation of sulfur at stainless steel surfaces, Electrochem. Sci. Technol. (1980) 27–30.
[8] D.W. Shoesmith, P. Taylor, M.G. Bailey, D.G. Owen, The formation of ferrous monosulfide polymorphs during the corrosion of iron by aqueous Hydrogen sulfide at 21 °C, J. Electrochem. Soc. 127 (1980) 1007–1015.
[9] C. Ren, D. Liu, Z. Bai, T. Li, Corrosion behavior of oil tube steel in simulant solution with hydrogen sulfide and carbon dioxide, Mater. Chem. Phys. 93 (2005) 209–305.
[10] A. Anderko, P.J. Shuler, A computational approach to predicting the formation of iron sulfide species using stability diagrams, Comput. Geosci. 23 (1997) 647–658.
[11] K. Choi, S. Kim, Morphological analysis and classification of types of surface corrosion damage by digital image processing, Corros. Sci. 47 (2005) 1–15.
[12] S. Laroche, C. Forget, Grain sizing of anodized aluminum by color image analysis, Mater. Charact. 36 (1996) 203–211.
[13] A.C. Lewis, J.F. Bingert, D.J. Rowenhorst, A. Gupta, A.B. Geltmacher, G. Spanos, Two-and three-dimensional microstructural characterization of a super-austenitic stainless steel, Mater. Sci. Eng. A 418 (2006) 11–18.
[14] J.C. Oliveira, A. Cavaleiro, C.M. Brett, Influence of sputtering conditions on corrosion of sputtered W-Ti-N thin film hard coatings: salt spray tests and image analysis, Corros. Sci. 42 (2000) 1881–1895.
[15] C. Punckt, M. Bölscher, H.H. Rotermund, A.S. Mikhailov, L. Organ, N. Budiansky, J.R. Scully, J.L. Hudson, Sudden onset of pitting corrosion on stainless steel as a critical phenomenon, Science 305 (2004) 1133–1136.
[16] J. López De La Cruz, M.A. Gutiérrez, Spatial statistics of pitting corrosion patterning: quadrat counts and the non-homogeneous Poisson process, Corros. Sci. 50 (2008) 1441–1448.
[17] J. López De La Cruz, R.H. Lindelauf, L. Koene, M.A. Gutiérrez, Stochastic approach to the spatial analysis of pitting corrosion and pit interaction, Electrochem. Commun. 9 (2007) 325–330.
[18] F.M. Pereira, M.I. Bueno, Image evaluation with chemometric strategies for quality control of paints, Anal. Chim. Acta 588 (2007) 184–191.
[19] Standard test methods for determining average grain size using semiautomatic and automatic image analysis, in: ASTM E 1382-97, NTU, 1997, pp. 855–878.
[20] C.B. Frederick, E.S. Daniel, Improved metallographic etching techniques for stainless steel and for stainless steel to carbon steel weldments, Metallography 9 (1976) 91–107.
[21] B. Reddy, B. Chatterji, An FFT-based technique for translation, rotation, and scale-invariant image registration, IEEE T. Image Process. 5 (1996) 1266–1271.
[22] L.L. Shreir, Corrosion of Metals and Alloys, vol. 1, Wiley Interscience, New York, 1978.
[23] F. Leander, L. Douglas, ASM Handbook, Metallography and Microstructures, in: ASM International, ASM International, 2004, p. 1020.
[24] H. Huang, W. Tsai, J. Lee, Electrochemical behavior of the simulated heat-affected zone of A516 carbon steel in H_2S, Electrochim. Acta 41 (1996) 1191–1199.
[25] M. Veloz, I. Gonzalez, Electrochemical study of carbon steel corrosion in buffered acetic acid solutions with chlorides and H_2S, Electrochim. Acta 48 (2002) 135–144.
[26] E. Behara, Metallographic reagents based on sulfide films, Practical Metallogr. 7 (1970) 242–248.
[27] E. Behara, B. Shpigler, Color Metallography, American Society for Metals, Metals Park, Ohio, 1977.
[28] E. Hansson, M. Odziemkowski, R. Gillham, Formation of crystalline iron monosulfides: surface redox reactions on high purity iron, spectroelectrochemical studies, Corros. Sci. 48 (2006) 3767–3783.
[29] S. Arzola, J. Genesca, The effect of H_2S concentration on the corrosion behavior of API 5L X-70 steel, J. Solid State Electr. 9 (2005) 197–200.
[30] E. Sosa, R. Cabrera-Sierra, M.T. Oropeza, F. Hernández, N. Casillas, R. Tremont, C. Cabrera, I. González, Electrochemical grown passive films on carbon steel (SAE 1018) in alkaline sour medium, Electrochim. Acta 48 (2003) 1665–1674.
[31] O. Marques Filho, H. Vieira Neto, Processamento Digital de Imagens, Rio de Janeiro-RJ, Brasport, 1999.
[32] R.C. Gonsalez, R.E. Woods, S.L. Eddins, Digital Image Processing using MATLAB, Pearson Education, 2004.
[33] M. Alshamasin, R. Al-kasasbeh, A. Khraiwish, Y. Al-shiboul, D.E. Skopin, Acceleration of image processing using new color model, Am. J. App. Sci. 6 (2009) 1015–1020.